Planetary and Space Science 86 (2013) 33–44

Contents lists available at ScienceDirect

Planetary and Space Science

journal homepage: www.elsevier.com/locate/pss

Numerical modelling of impact crater formation associated with isolated lunar skylight candidates on lava tubes

E. Martellato [a,*], B.H. Foing [a,b], J. Benkhoff [a]

[a] ESA/ESTEC-SRE-S, Keplerlaan 1, 2201 AZ Noordwijk ZH, The Netherlands
[b] Vrije Universiteit Amsterdam, Faculty of Earth and Life Sciences, De Boelelaan 1085, 1081 HV Amsterdam, The Netherlands

ARTICLE INFO

Article history:
Received 16 October 2012
Received in revised form
13 June 2013
Accepted 16 June 2013
Available online 22 June 2013

Keywords:
Moon
Numerical modelling
Impact craters
Skylights
Lava tubes
Space exploration

ABSTRACT

Skylights are openings on subsurface voids as lava tubes and caves. Recently deep hole structures, possibly skylights, were discovered on lunar photo images by the JAXA SELenological and ENgineering Explorer (SELENE)-Kaguya mission, and successively confirmed by the NASA Lunar Reconnaissance Orbiter (LRO) mission. Vertical hole structures and possibly underlying subsurface voids have high potential as resources for scientific study, and future unmanned and manned activities on the Moon. One mechanism proposed for their formation is impact cratering. The collapse of craters is due to the back spallation phenomena on the rear surface of the lava tube roofs. Previous analysis in this topic was based on small-scales laboratory experiments. These have pointed out that (i) the target thickness-to-crater diameter ratio is 0.7, and (ii) the projectile diameter-to-target thickness ratio is 0.16, at the ballistic limit once extrapolated to planetary conditions.

We investigate the impact process that might trigger the formation of lunar skylight candidates by numerically simulate the craters associated to the observed hole structures. The Marius Hills hole (MHh, located in a 26 m thick target) was formed by a 4 m projectile, which originated an impact crater of 40.0 ± 1.6 m in diameter. The Mare Tranquillitatis hole (MTh, located in a 47 m thick target) was formed by a 7.2 m projectile, which originated an impact crater of 75.6 ± 3.0 m in diameter. The target thickness-to-crater diameter ratio is 0.65 and 0.62, respectively for MHh and MTh. These values are smaller than the laboratory experiment ballistic limit ratio (0.7), supporting the hypothesis of collapse at the studied sites. The projectile diameter-to-target thickness ratio is 0.15 for both MHh and MTh, which is slightly smaller than we expected. The discrepancy could be due to the model assumption of vertical impact. We derived via modelling the ballistic limit for planetary scales and found that the target thickness-to-crater diameter ratio is 0.87.

We discuss the implications of the proposed scenario for skylight formation in terms of future robotic or human exploration of the Moon, as evaluated in COSPAR and ILEWG.

1. Introduction

Skylights are apertures on underground structures, such as lava tubes or caves (e.g., Calvari and Pinkerton, 1999). The terrestrial skylights expose the incandescent lava flowing inside lava tubes, which are conduits that develop by radiative cooling a solid crust whereas the lava stream below is still liquid and flowing away from the feeding vent (e.g., Greeley, 1971; Keszthelyi, 1995). Lava tubes are common on the basalt flows on the Earth, but also in similar terrains on the Moon and Mars (e.g., Cruikshank and Wood, 1972), since such features are lastly controlled by the rheological properties of lavas and mechanisms of eruption and emplacement. On the Earth, the best examples are given by Mauna Loa, Mauna Ulu, and Etna volcanoes (e.g., Greeley, 1987), where skylights have been found in all these environments (e.g., Okubo and Martel, 1998; Calvari and Pinkerton, 1999). Skylights often form as graben-like trenches due to gravitational collapse of lava tubes roofs after volcanic activity ceased (e.g. Cruikshank and Wood, 1972).

Terrestrial skylights have been deeply studied through both on field investigation and satellite data. The connexion of these strategies of investigation has advantages for the other planetary contexts. In fact, it is important to understand how skylights look like in space images of the Earth, where they are positively identified. A similar morphology is then considered as reference for searching skylights in terrestrial planets and discriminating them to other endogenic or exogenic structures. These landforms

* Corresponding author. Tel.: +39 0715655352; fax: +39 0715654697.
E-mail addresses: emartell@rssd.esa.int, elena.martellato@oapd.inaf.it (E. Martellato).

0032-0633/$ - see front matter © 2013 Elsevier Ltd. All rights reserved.
http://dx.doi.org/10.1016/j.pss.2013.06.010

reveal to be in turn the primary method for locating lava tubes, whose widespread in time and space is extremely important for a global comprehension of volcanism and the thermal evolution of the other terrestrial planets.

In this way, skylights have been observed on Mars and the Moon and a plethora of works has been published about hole structures located in very different geological contexts (e.g., Cushing et al., 2007; Greeley and Gault, 1979; Haruyama et al., 2009, 2010, 2012; Okubo and Martel, 1998; Robinson et al., 2012). These structures have been addressed either as *pit craters* (e.g., Okubo and Martel, 1998) or *basaltic collapsed depressions* (e.g., Greeley and Gault, 1979), causing some general misunderstanding. Indeed "pit crater" has been adopted either for cone-shaped structures produced by dilational normal faulting and sub-vertical fissuring (e.g., Wyrick et al., 2004), and for arcuate shaped hollows located on smooth deposits within Hermean peak-ring basins possibly related to explosive volcanism (e.g., Gillis-Davis et al., 2009). "Collapsed depression" refers mainly to gravitational collapse affecting roofs of lava tubes and caves. However, such a collapse is not the only mechanisms responsible of hole structure formation on planetary surfaces, being impact on lava tube roofs another likely process. Different mechanisms can be indeed envisaged whether skylights are found isolated or in chain. Hence, hereinafter, we will not consider the terms "pit craters" and "collapsed depressions" in order to avoid possible misunderstanding, and we will favour terms as "skylight candidates" or "hole structures", which do not refer to any genetic process.

In the extraterrestrial environments, skylights should display a distinguishable morphology with respect to exogenic structures, as they have no raised rim, sloped wall, visible floor or detectable extended ejecta blanket (e.g., Cushing et al., 2007). For instance, on Mars, Cushing et al. (2007) reported skylight candidates on and around the flanks of Arsia Mons. Such landforms are detected as dark flat hollows on planetary images in the visible range, or as thermal anomalies with respect to the surroundings on infrared data (Cushing et al., 2007; Léveillé and Datta, 2010). They could be found in chain and with irregular shapes (e.g., Robinson et al., 2012; Wyrick et al., 2004), and are considered as landmarks to possibly localise lava tubes (Léveillé and Datta, 2010). These underground caves have conditions very different from the surface environment, and therefore they keep a unique and uncommon role as place where past geologic and climate history is preserved and are perfect candidates for life quest on Mars (Barton, 2006; Boston et al., 1992).

On the Moon, several lunar skylight candidates were only recently recognised on images acquired by the Terrain Camera (TC) onboard SELENE-Kaguya (Haruyama et al., 2009, 2010), and then confirmed on the higher resolution images acquired by the Lunar Reconnaissance Orbiter Camera (LROC) on-board LRO (Robinson et al., 2012). They are very likely associated with lava tubes (e.g., Haruyama et al., 2009), which had an important role in lava emplacement within basaltic lunar maria (e.g., Haruyama et al., 2012).

The first detected skylight candidate is located in the Marius Hills region within Oceanus Procellarum (Fig. 1a), in a region of the Moon with high volcanic activity (e.g., Haruyama et al., 2009). Other skylight candidates have been observed in Mare Tranquillitatis (Fig. 1b), and Mare Ingenii, both in regions quite far from peculiar volcanic or tectonic landforms (Robinson et al., 2012). Further skylight candidates were detected in impact melt deposits, where they might point to plumbing networks (Robinson et al., 2012). These features are slightly elliptical to irregular lobate shaped and are characterised by several layers (up to eight layers identified), with a thickness ranging between 1 and 14 m at the hole walls and flat floors covered by a cohesionless diamicton with boulders' length between 1 and 8 m. The sequence of bed-rocks

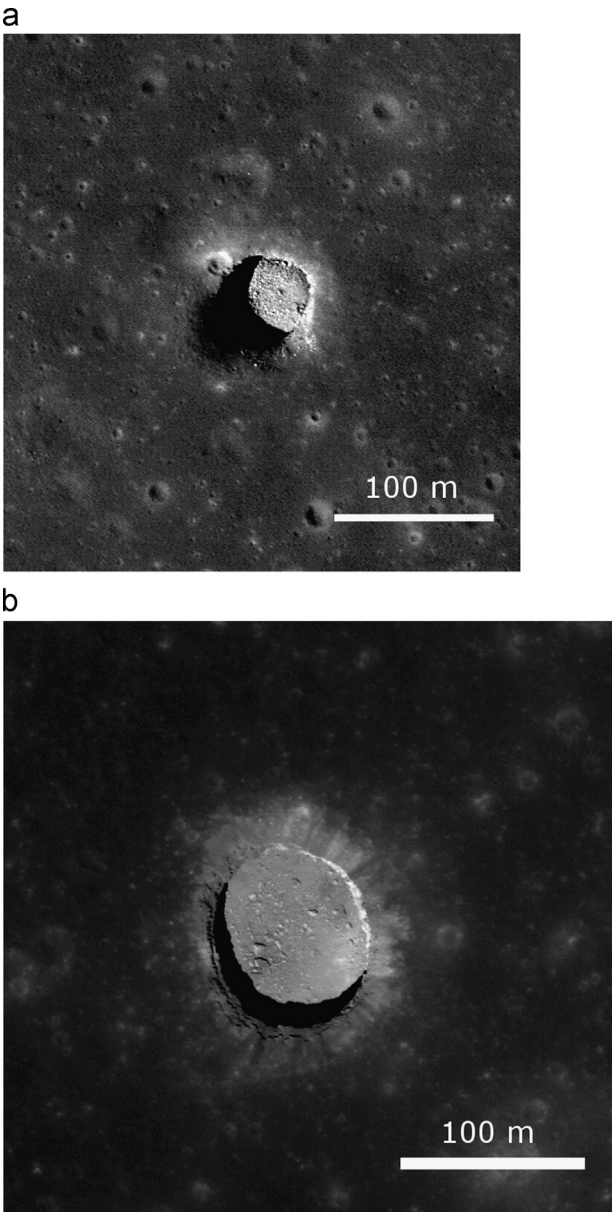

Fig. 1. a. Marius Hills skylight (MHh) is located in the Marius Hills region of Oceanus Procellarum at 14.2°N and 303.3°E. This image is the M122584310L of the LROC database. It has a resolution of 0.5 m/px, an emission angle of 1.67° and an incidence angle of 25.08°. (b). Mare Tranquillitatis skylight (MTh) is located within the basaltic blanket of Mare Tranquillitatis at 8.3°N and 33.2°E. This image is the M155016845R of the LROC database. It has a resolution of 0.5 m/px, an emission angle of 4.85° and an incidence angle of 10.58°.

layers interleaved by thin weak regolithic soils forms stair case topographic profiles at the skylight walls. This might suggest subsequent flow events after lava tube formation, each ones separated by a period of time long enough to form soil layers.

Both MHh and MTh are slightly elliptical. MHh has a diameter value ranging from 49 to 57 m, while MTh has a diameter ranging from 86 to 100 m (Robinson et al., 2012). LROC Narrow Angle Camera (NAC) oblique images pointed to a cavernous nature for either MHh or MTh, defined by a wall with a finite thickness over a void space. Shadow measurements and stereo-derived digital terrain models allow to infer the maximum floor depths from the lunar surface, which are 43 m and 107 m, respectively for the two holes (Robinson et al., 2012). NAC oblique images give the heights of the roof above the cave floors. The results are of 17 m and 60 m,

Table 1
Skylight candidates detected so far in LROC and TC images.

	Coordinates[a]	diameter (m)		depth (m)	roof's thickness (m)[a]
		range values	mean value[a]		
Marius Hills hole	14.1°N, 303.2°E	49–57[a] 50–59[b]	53	43[c] 40–44[d] 48[b]	26
Mar Tranquillitatis hole	8.3°N, 33.2°E	86–100[a] 84–98[b]	93	107[c] 107[b]	47
Mare Ingenii hole	35.95°S, 166.06°E	71–104[a] 68–118[b]	87.5	39–64[c] 38–67[d] 45[b]	37
King pond bridge	6.24°N, 10.33°E	24–56[a]	40	11[c]	—
Copernicus pond pit	10.33°N, 339.62°E	50–90[a]	70	23[c]	—

[a] Robinson et al. (2012).
[b] Haruyama et al. (2012).
[c] Depths from shadow measurements in Robinson et al. (2012).
[d] Depths measured with stereogrammetric techniques Robinson et al. (2012).

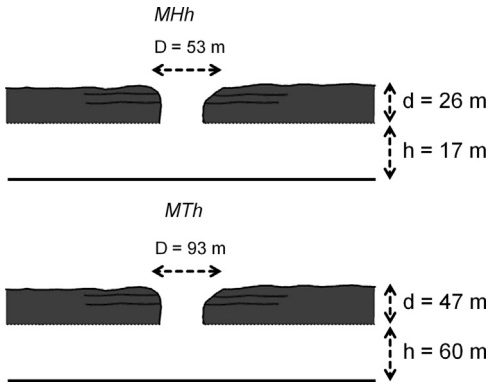

Fig. 2. Schematic representation of the two skylights geometries with the measurements given by Robinson et al. (2012) and adopted in this paper for our investigation: Marius Hills hole (above) and Mare Tranquillitatis hole (bottom).

respectively for the MHh and MTh caves (Robinson et al., 2012). We summarise the main characteristics of the detected skylight candidates in Table 1, whereas in Fig. 2 we show the geometries and related values of the two skylights investigated in this study.

Terrestrial and planetary skylights could originate as structural failure due to the weight of the roof when magma withdrawals at depth (e.g., Greeley and Gault, 1979; Wentworth and MacDonald, 1953), enlargement of pre-existing fractures (Greeley, 1970), incomplete crusting over the melted lava flow (e.g., Calvari and Pinkerton, 1998), or in response to the stoping emplacement above rift zone fractures (Okubo and Martel, 1998). Nevertheless, it is worthy to mention that, whatever the forming process is, skylights are likely a later landform, as they are not usually surrounded by either flows or pyroclastic debris, which are the signature for primary vents of effusive and explosive eruptions, respectively (Okubo and Martel, 1998).

Another mechanism, which is more likely for skylights on Mars and the Moon, but at the same time keeps the connotation of a later stage, is the collapse of roofs of lava tubes or caves caused by random meteoroid impacts (e.g., Coombs and Hawke, 1992; Hörz, 1985; Oberbeck et al., 1969). In this case, the collapse at the origin of a skylight is caused by an impact on a lava tube roof whose thickness is unable to handle the effects of the propagating shock waves. Oberbeck et al. (1969) firstly proposed the idea that collapsed section of lava tubes could form through meteoroid erosion. Successively, Hörz (1985) resumed the impact cratering hypothesis to assess the stability of lava tubes as suitable human settlements on the Moon. Hörz (1985) used previous experimental studies on slab-like targets to suggest that the roof of any lava tube should be at least two times larger than the larger crater depth to not collapse. Skylights analysis and a possible related impact origin have been then re-evaluated more recently when skylights candidates were detected on SELENE-Kaguya TC (Haruyama et al., 2009, 2010, 2012) and LROC (Robinson et al., 2012) images.

The collapse after a random impact could not nevertheless be invoked as feasible formation mechanism for those skylights occurring in chains or displaying irregular shapes (e.g., Cushing et al., 2007). Hence, since we want to explore the reliability of this process, in the following we will refer only to isolated elliptical-shaped skylight candidates, i.e. MHh and MTh. Indeed Mare Ingenii case and holes on impact melt deposits show irregular shapes possibly driven by a gravitational collapse or by a structural control of pre-existing anisotropies on the impact crater shapes.

In this paper, we aim to investigate impact cratering as formation mechanism for skylights, and the conditions that permit the development of a hole from a given impact crater, considering the physical setting of MHh and MTh. In the next two sections, we will focus on spallation on slab-like targets from the small-scale experiment (Section 2) and numerical modelling (Section 3) approaches. In Section 4, we will present and discuss the results obtained from the numerical simulations performed to study MHh and MTh, and we derived the threshold target thickness-to-crater diameter ratio for the collapse. Finally, in Section 5 we will report the conclusion of our study, and its contextualisation on the lunar exploration programme.

2. Recent small-scale laboratory experiments

When a meteoroid (projectile) strikes the surface (target), the rapid compression of both materials causes the formation of shock waves that rapidly expand and attenuate through the target (e.g., Melosh, 1989). As soon as shock encounters a free surface, it is reflected back as a tensile rarefaction wave and causes fracturing and shattering of the target rocks beneath the impact

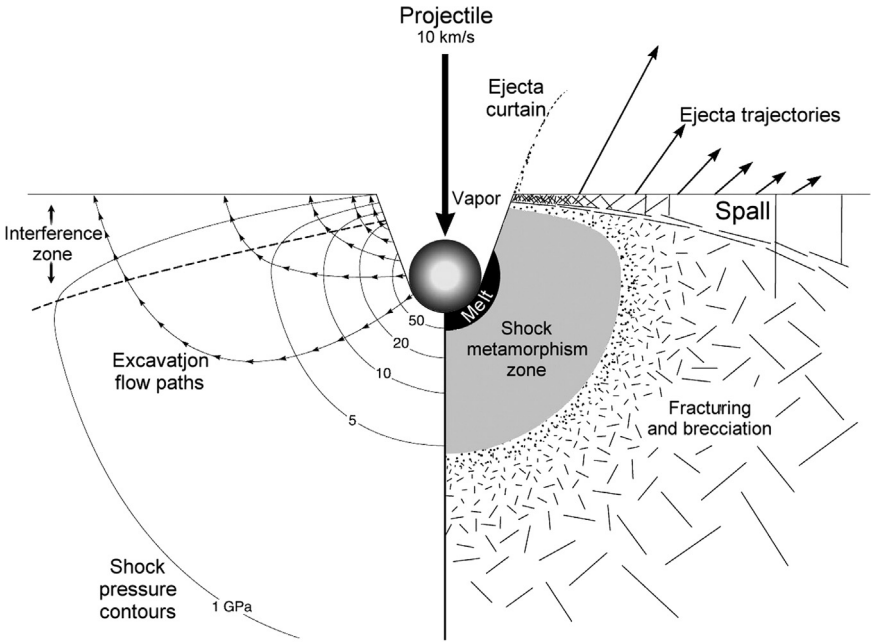

Fig. 3. Illustration of excavation the excavation stage, when the spallation phenomena occur due to the tensile failure of target and to the ejection of lightly shocked material. Modified after French (1998).

crater. Target rocks nearby the growing crater undergo damage after the applied stresses exceed shear or tensile strength (e.g., Kenkmann and Ivanov, 2006). Shock and rarefaction waves onset target material in motion to begin the excavation flow responsible of the opening of a transient cavity, which then develops into the final crater (Fig. 3). However, near free surfaces, pressures do not get high values, because they are limited by the interference between shock and rarefaction waves. Hence, the target material within this region surrounding the impact site is lightly shocked (Melosh, 1984, 1989).

Spallation relies on the fragmentation and ejection of such near-surface coherent material parallel to the wave front, resulting from the dynamic tensile failure along a perpendicular plan, due to the interaction between the direct compression and the reflected rarefaction waves (e.g., Dufresne et al., 2013; Johnson, 1981; Melosh, 1984; Polanskey and Ahrens, 1990). Spall damage in brittle materials occurs throughout the nucleation, growth, and coalescence of cracks, due to stresses exceeding the tensile strength of the material, but without large-scale plastic deformation (Davison and Graham, 1979; Johnson, 1981). The spall thickness was defined by Melosh (1984) as the depth at which the tensile stress reaches the dynamic tensile strength of the target material (cf. Eq. (14) in Melosh, 1984). The tensile stress required to produce some given level of damage is called the spall strength, which depends on the degree of damage taken to form a spall and the duration of the tensile stress pulse (Davison and Graham, 1979). The high pressure gradient in the near-surface region accelerates the spall fragments to velocities comparable to the impact velocity itself (e.g., Melosh, 1984).

In finite-size targets, the expanding shock wave is reflected at the rear surface too, giving rise to multiple rarefaction waves, which influence the growth of the crater and enhance damage effects close by the cavity (e.g., Fujiwara, 1980; Hörz, 2012; Hörz et al., 1995). Fracture systems observed in impact experiments consist of a hemispherical area right beneath the crater, which is characterised by a high density of small *shear* fractures, together with *radial* and *concentric* fractures. On the other hand, *sub-horizontal* fractures associated to the *tension* failure are found below and parallel to the floor of the proposed spalled zone (Figs. 4 and 5 in Polanskey and Ahrens, 1990). Similar results were also obtained in numerical modelling investigations (e.g., Ivanov et al., 1997; Kenkmann et al., 2011). Thick targets can undergo the formation of rear bulges and internal delaminations (Hörz, 2012), and targets twice as thick as the impact crater depth could be perforated (Hörz et al., 1995) due to back spallation.

Experiments in variable thickness (T) Teflon and Al_{1100} targets were performed by Hörz et al. (1995) and Hörz (2012). Soda-lime glass (SGL) projectiles with diameters (D_p) between 0.5 and 3.2 mm were impacted at velocities of 1–7 km/s to study the transition from cratering ($D_p/T \ll 1$) to perforation. Standard craters (with diameter D_c) forming in thick targets showed a velocity-dependent morphology, with a higher depth/diameter ratio in the case of low-velocity projectiles (<2 km/s). On the other hand, at higher velocities (>5 km/s), the depth/diameter ratio remained quite approximately 0.58. At increasing D_p/T ratio (0.33 and 0.16, respectively for 4.0 and 6.7 km/s impact velocities), bulging and spallation at the rear target surface were detected. Hörz et al. (1995) and Hörz (2012) defined the spall diameter as the diameter of highly scalloped spall zone surrounding the crater. The threshold to the penetration regime, called ballistic limit, was velocity-dependent too and the corresponding D_p/T ratio ranged from 0.65 to 0.33 for velocities of 2 and 6 km/s, respectively. The extrapolation of the laboratory data to lunar-like impact velocities led the D_p/T ratio at the ballistic limit to be approximately 0.16, or equally the T/D_c ratio to be about 0.7 (cf. Fig. 13 in Hörz, 2012).

Gehring (1970) performed experiments using 3.18-mm Al spheres impacting at 7.4 km/s in Al slab-like targets with thickness ranging between 1.0 and 5.1 cm. Concerning the impact structures, the results of laboratory experiments by Gehring (1970) showed that the thickness of the target should be about 2.1 times the depth of a crater to prevent spall, and about 1.7 to prevent perforation.

Porosity plays an important role in the propagation of the shock front, whose energy is spent into target heating, spallation, disruption, and crushing of the grains to fill the void spaces (e.g., Love et al., 1993). Crater volumes and cratering efficiency are thus reduced by porosity (e.g., Poelchau et al., 2013). On the other hand, porous materials are low in cohesion and compressive yield

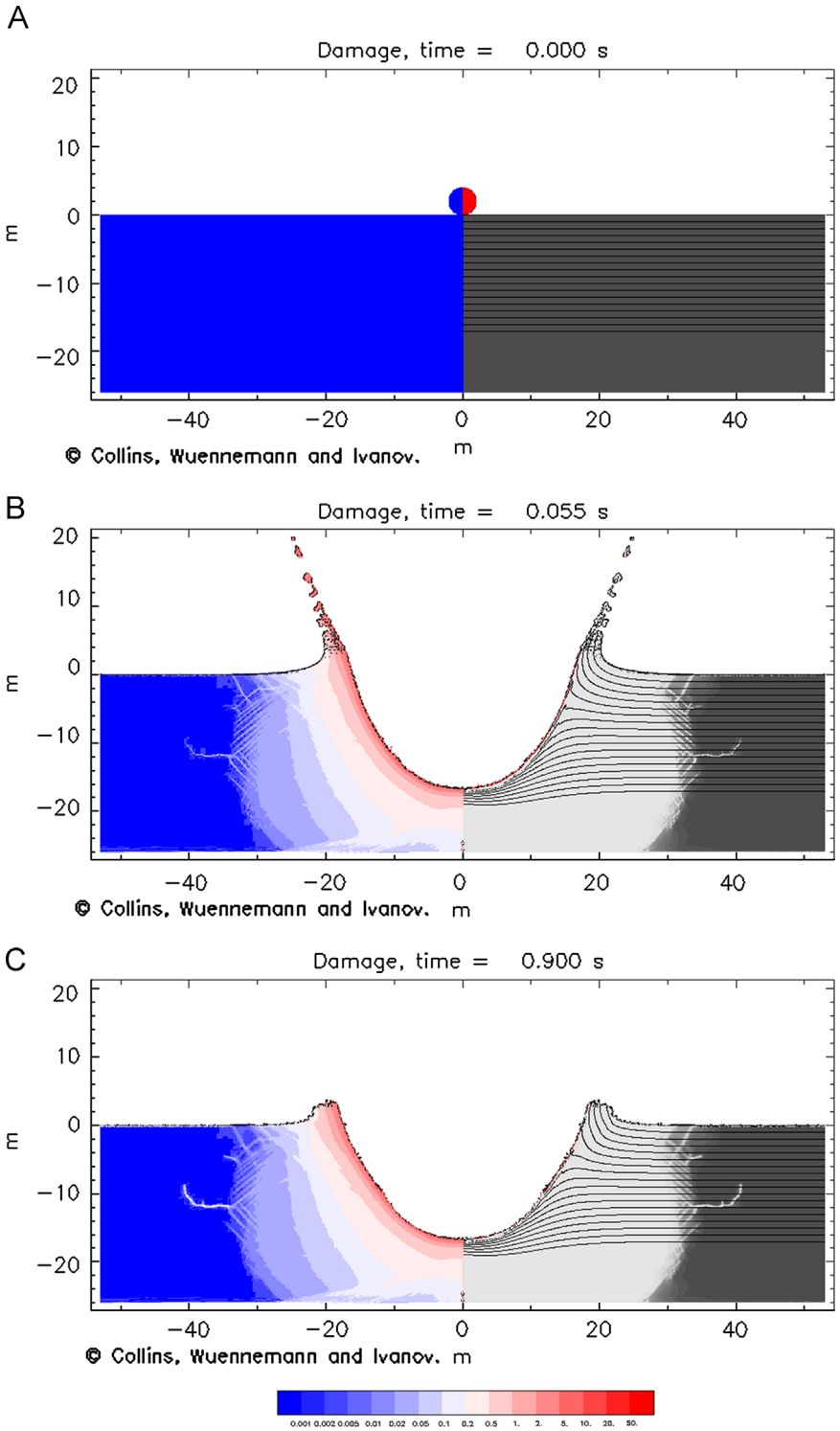

Fig. 4. Snapshots of the computer simulations of the impact crater, whose subsequent collapse stood at the origin of Marius Hills hole. The right panel of each plot represents the amount of damage on a grey scale, where white corresponds to the maximum level of damage. The left panel depicts the distribution, for the same cross section, of the total plastic strain (TPS) that was accumulated during the passage of the shock wave and subsequent crater formation (red: high TPS; blue: low TPS). (For interpretation of the references to color in this figure legend, the reader is referred to the web version of this article.)

strength. Love et al. (1993) let a 1.6 mm SLG projectile impact at 6 km/s into loosely bonded solid aggregate targets, with porosities between 5 and 60%, in order to explore the effects of porosity on cratering into slab/like targets. They barely found backside spallation in those targets with higher porosity, confirming the poor transmission of shock energy because of the extreme acoustic impedance mismatches between solid and void components in porous targets. Their experiments suggested an increase of the penetration depth with increasing porosity.

More recently, the Multidisciplinary Experimental and Modeling Impact Crater Research Network (MEMIN) research unit has investigated the effect of variables such as projectile velocity and mass and target pore space saturation throughout a series of small scale experiments into sandstone (Dufresne et al., 2013; Kenkmann et al.,

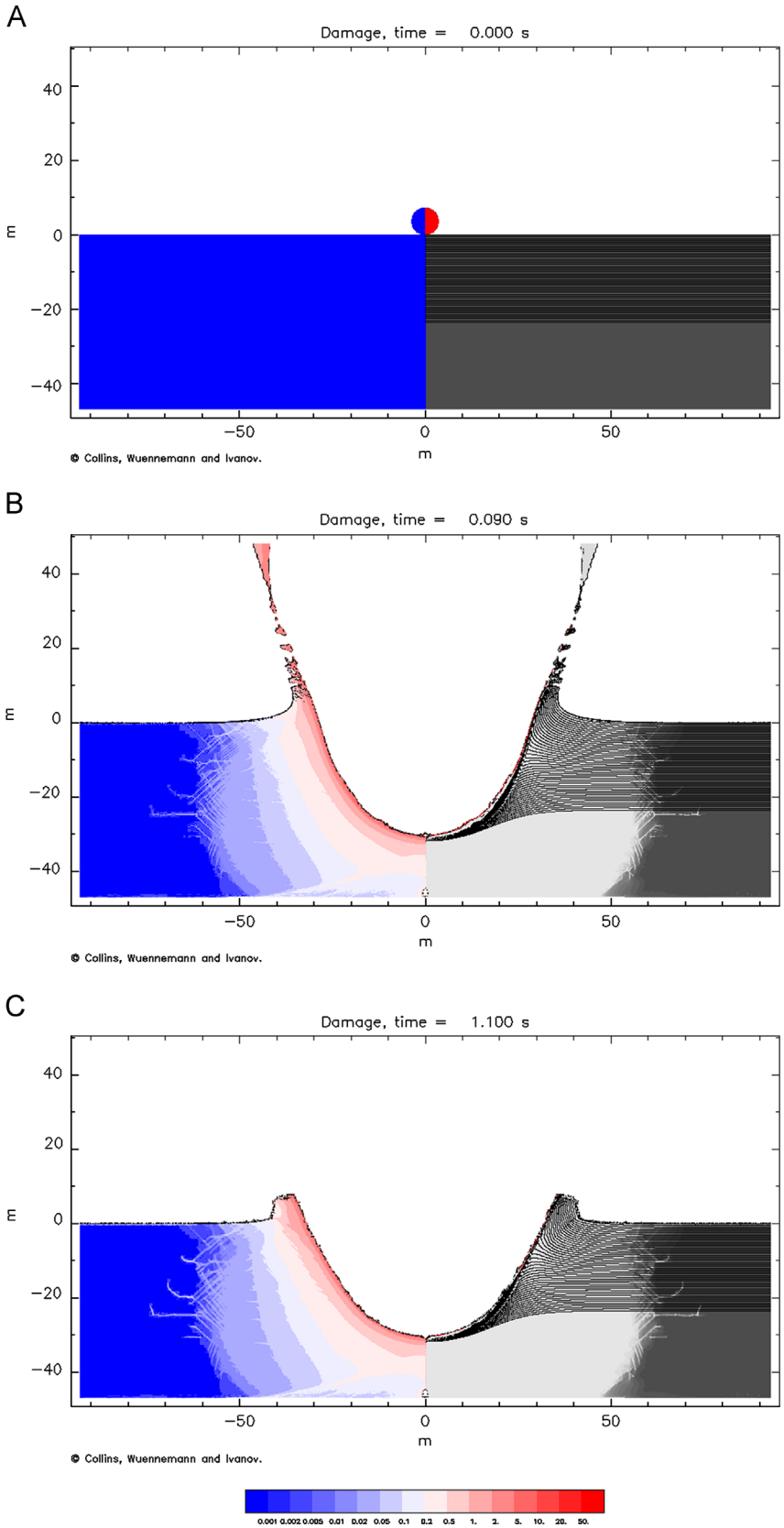

Fig. 5. Snapshots of the computer simulations of the impact crater that triggered the formation of Mare Tranquillitatis hole. As in Fig. 4, the right panel shows the extension of the material damage, while the left panel the TPS contours. The colour legend is the same as in Fig. 4. (For interpretation of the references to color in this figure legend, the reader is referred to the web version of this article.)

2011; Poelchau et al., 2013). Projectiles are steel and aluminium spheres, or iron meteorites, with diameters ranging between 2.5 and 12 mm, while impact velocity is of 2.5 up to 7.8 km/s. Poelchau et al. (2013) observed that the penetration depth and the

resulting depth/diameter ratio strongly increased with increasing porosity. Dufresne et al. (2013) observed that the final crater had a central highly fragmented depression, surrounded by an outer spallation zone which was beginning at the crater rim. When 90% water-saturated targets were adopted, the crater exhibited pronounced concentric topographic steps in the outer spallation zone with respect to a 10°–20° sloped surface. Poelchau et al. (2013) finally pointed to an enhancement of spallation in larger-scale experiments, and a consequent increasing of cratering efficiency with increasing projectile size.

3. Numerical modelling

Impact cratering is mostly studied via observation of craters, theory, and laboratory experiments. Only few impact events have been directly observed. These are comet Shoemaker–Levy 9 on Jupiter (e.g. Levy, 1998), and artificial impactors, such as Deep Impact on comet Temple I (e.g., Richardson et al., 2005), and SMART-1 and LCROSS on the Moon (e.g., Burchell et al., 2010; Korycansky et al., 2009; Schultz et al., 2010). Nevertheless, over the last few decades, rapid improvement of computer capabilities has allowed numerical modelling to become a powerful tool in studying impacts, because it can simulate conditions beyond the reach of experiments (e.g., velocity, size) (e.g., Pierazzo and Collins, 2004), and it allows to investigate the complexity of crater collapse on planetary scale (e.g., Collins et al., 2002). It can also help in outlining the individual effect of any variable in the model, such as porosity or internal friction (e.g., Elbeshausen et al., 2009; Wünnemann et al., 2006), and in understanding the physics of the process.

Numerical modelling is performed throughout shock codes, which handles the formation and propagation of shock waves, as well as the behaviour of geologic materials over a broad range of stress states and of deformation rates (Anderson, 1987; Pierazzo et al., 2008). Over the years, a number of shock codes has been developed and refined, and each one could compute the state variables by implementing different approaches to solve the dynamics of shock wave propagation, and by adopting different constitutive equations (e.g., Pierazzo et al., 2008). Our group is using iSALE (impact Simplified Arbitrary Lagrangian Eulerian) shock physics code (e.g., Amsden et al., 1980; Collins et al., 2004; Ivanov et al., 1997; Melosh et al., 1992; Wünnemann and Ivanov, 2003; Wünnemann et al., 2006).

The original code, i.e. SALE, was developed by Amsden et al. (1980) for simulating single-material Newtonian-fluid flow, by using either, or a combination, of the Lagrangian and Eulerian descriptions. This code included no failure model and simple equation of states (EoS) and constitutive model. Hence, to simulate hypervelocity impact processes in solid material, SALE has been modified to include extensions, correction and enhancements, giving rise to a "family" of SALE extensions.

The first extended release was SALEB, a simple versatile hydrocode, capable of simulating impact events from the first contact of the impactor with the target, to cessation of the final gravity driven collapse of the craters (e.g., Ivanov, 2005; Ivanov and Artemieva, 2002). Melosh et al. (1992) implemented an elasto-plastic constitutive model in tandem with the viscous model, and incorporated the Grady–Kipp fragmentation algorithm and several equations of state for impacts, including the Tillotson equation of state (Tillotson, 1962). Ivanov et al. (1997) advanced the underlying solution algorithm by incorporating free-surface and material-interface tracking in Eulerian mode, improved the constitutive model by incorporating damage accumulation and strain-weakening, and implemented into the code the semi-analytical equation of state ANEOS (Thompson and Lauson, 1970, 1972).

A second release was SALES-2, in which the Melosh's Lagrangian version of the original SALE was improved to include a wider range of possible rheological models (Collins et al., 2002).

A further release was iSALE. The major improvements of this version were significant changes to the code needed to perform simulations in pure Eulerian mode (Wünnemann & Lange, 2002), the introduction of a third target material (Wünnemann & Ivanov, 2003; Wünnemann et al., 2005), refinements to the constitutive model (Collins et al., 2004), and the incorporation of the ε–α porous-compaction model (Collins et al., 2011b; Wünnemann et al., 2006). More recently, a routine has been added to construct a self-consistent central gravity field for the simulation of giant impacts onto spherical planetary bodies (Davison et al., 2010).

iSALE is well tested against laboratory experiments at low and high strain-rates (Wünnemann et al., 2006), and other hydrocodes (Pierazzo et al., 2008). In particular, Pierazzo et al. (2008) reported an exhaustive work of benchmark and validation of a number of shock codes widespread among the impact community. The benchmark tests aimed at quantifying the dissimilarities between hydrocodes due to differences in the underlying solution algorithm, artificial stability parameters, and material models characteristics of each code. They found that the shock pressures obtained by the considered hydrocodes vary from 8% to 15%, depending on the impact conditions. The validation tests focused on assessing the accuracy of hydrocodes to reproduce laboratory impacts into water and aluminium alloys. They found that the model results agree within 15–20% with experiments. In particular, depending on the material model adopted, iSALE underestimates the final crater radius by $\sim$3–5%, and overestimates crater depth by $\sim$12% with respect to experiments (Pierazzo et al., 2008).

iSALE is a two-dimensional hydrocode that employs axial symmetry. This limits impact events to normal incidence angles, and collisional events to a head-on, direct impact geometry. The duration of each simulation was long enough to follow the generation, propagation and release of shock waves in each collision, until the completion of the crater.

To develop a consistent model for MHh and MTh, we adopt a head-on impact with the projectile hitting perpendicularly onto the target surface. This configuration is forced by the axisymmetric nature of the model (e.g., Collins et al., 2008a). The overall mesh is made up by a high resolution zone in the proximity of the impact site, respectively of 530×700 and 930×950 cells for the two cases. In the right boundary, this area is in turn followed by a zone of progressively lower resolution, where the cell size is increased by a factor of 1.05 from the previous cell, in order to mitigate spurious effects coming from the interference between the "real" shock wave and the "false" reflection wave at the grid boundaries. This extension is not imposed at the bottom boundary of the mesh, because we right aim to investigate the effects of back-spallation occurring in a slab-like target when shock waves interfere with the rarefaction waves coming from the rear surface. The target is chosen of basaltic composition to better describe the solidified magma, with thickness given in Fig. 2. Porosity is fixed to 7.7% after Huang and Wieczorek (2012). They derived this value by combining lunar gravity and topography profiles with a lithospheric model that included both surface and subsurface loading.

The projectile is chosen to be of asteroidal origin, which is the most likely impactor population on the Earth–Moon system ($>$90%; Chyba, 1991; Pierazzo and Chyba, 1999). We consider basalt as well to describe the impactor composition, with a porosity of 10%, which is derived from the average of the meteorite types proposed by Britt et al. (2002) (cf. Table 2 in Britt et al., 2002). The thermodynamic behaviour of basalt is described by the ANalytical Equation Of State (ANEOS) (Thompson, 1970; Thompson and Lauson, 1972). The strength model used in the numerical simulations is the standard rock strength algorithm implemented

Table 2
Numerical model parameters.

Symbol	Definition	Value	
GRID:		**530 × 700 (MHh), 930 × 950 (MTh)**	
		Projectile:	**Target:**
R	Projectile radius	12, 20, 36 CPPR	
v_i	Impact velocity	18 km/s	
t	Target thickness		26 m, 47 m
	Material	basalt	basalt
ρ_i, ρ_t	Material density	2.86 kg/m^3	2.86 kg/m^3
	Material porosity	10%	7.7%
Y_0	Cohesion (yield strength at zero pressure)	20 MPa	50 MPa
Y_m	von Mises plastic limit (yield strength at infinite pressure)	2.5 GPa	2.5 GPa
μ_i	Coefficient of internal friction	1.4	1.5
μ_d	Coefficient of friction (damaged material)	0.6	0.6
T_m	Melt temperature	1360 K	1360 K

in iSALE, which accounts for changes in material shear strength resulting from changes in pressure, temperature and both shear and tensile damage (Melosh et al., 1992; Ivanov et al., 1997; Collins et al., 2004).

The average impact velocity v_i on the Moon for small impactors is 18 km/s (Marchi et al., 2009). However, perpendicular impacts are not common in nature, being 45° the most probable angle of impact with respect to the target plane (e.g., Gault and Wedekind, 1978; Shoemaker, 1962). On the other hand, iSALE has a 2D capability that limits the studied impact events to normal incidence angles. Hence, we carried out our simulations implementing the full value of velocity, in order to evaluate the maximum effects for both impacts, and we refer to Section 4 for a discussion on the influence of the impact angle on the final results, as over 90% of all impacts are oblique (Collins et al., 2011a) and our structures are both elliptical in shape.

The impactors size has been firstly estimated with the scaling law given in Holsapple and Housen (2007), and derived in the gravity regime for sand or cohesive soils (cf. Table 1 in Holsapple and Housen, 2007). A series of runs at low resolution was aimed at constraining the projectile diameters for the various impacts considered in the analysis: the simulation of both MHh and MTh, and the assessment via numerical modelling of the ballistic limit for the target thickness at the site of the studied skylight candidates.

In Table 2, we report the summary of our model setting.

4. Results and discussion

Isolated skylights on planetary contexts have been deemed to form after the collapse of impact craters on lava tube or cave roofs (Hörz, 1985; Oberbeck et al., 1969). Since both MHh and MTh show no rim, the craters which formed these skylight candidates experienced collapse both on their floors and on their rims. As we could not know the real extent of such collapse, we hypothesise that such a collapse could be accounted for the widespread fracture system due to both shear and tension failures of the target material (e.g., Polanskey and Ahrens, 1990). This is because the fractured rocks are weaker than intact rocks (Collins et al., 2004), and hence they are more easily involved in further sliding than the surrounding intact rocks (Rice, 1976). Therefore, the observed hole structures could likely represent the damage area surrounding the original impact crater. In the following, we will refer with D_c and d_c as the impact crater diameter and depth, respectively, while D_{da} will be the extent of the damage area.

The results of small-scale laboratory in Teflon by Hörz (2012) pointed out that the spall-to-crater diameters ratio is slightly decreasing with higher velocity, and it is about 2.2 at 7 km/s (cf. Fig. 19 in Hörz, 2012). On the other hand, the extrapolation of laboratory data to planetary craters by Dufresne et al. (2013) led to propose that spall detachments in the Ries impact crater in Germany occur at 0.8–1.8 crater radii from the crater's centre, with mean value of 1.3. Both MHh and MTh have funnel-like slopes around the upper edges of the vertical walls of the holes. The spall diameters are thus possibly larger than the hole diameters given in Table 1. Therefore, we assume that the collapse is limited to the crater rim.

In the case of simple craters, the damage area extends up to about 1.5 crater radii from the crater's centre. This value is the average of the distance range where the rim drops to zero (Melosh, 1989). If the value of 1.5 is applicable for D_{da}/D_c, the related diameters of impact craters for MHh ($D_{c,\,MHh}$) and MTh ($D_{c,\,MTh}$) are estimated to be about 35 m and 62 m, respectively. The ratio of the target thickness-to-the diameter of craters (T/D_c) at the ballistic limit is 0.7, and given by Hörz (2012) for the case of small scale experiments (see Section 2). When we use this value, the threshold thicknesses to have perforation for MHh (T_{MHh}) and MTh (T_{MTh}) would be 24.5 m and 43.4 m, which are both almost same as, or a little bit lower than the observed lava tube roof thicknesses of 26 m and 47 m (cf. Table 1). As the observed roof thicknesses are required to be at least at the ballistic limit to account for the collapse, small scale experiments likely provide a good prediction for the roof thicknesses threshold of the possible lava tubes associated to the studied lunar hole structures, since they only slightly underestimate it.

We performed low resolution exploration to examine the formation of craters with damage area sizes as large as the lunar hole diameters. For the MHh case, we found that the possible projectile is 4 m in diameter. Fig. 4 shows the snapshots of the formation of the crater standing at the origin of MHh. The projectile transfers most of its kinetic energy into both kinetic and internal energy of the target material at the contact point (Fig. 4A). The internal energy is spent to either melt or even vaporise material in close proximity to the impact site, whereas the residual kinetic energy works to eject target material on ballistic trajectories and open the cavity. The culmination of the excavation stage is defined as the moment when the excavation flow ceases and halts the growth of the cavity (Fig. 4B). At this stage, the cavity is called transient crater, and could be approximated as a paraboloid of revolution with a depth-to-diameter ratio ranging between 1:3 and 1:4 (e.g., Grieve et al., 1989; Melosh, 1989; Melosh and Ivanov, 1999). The final crater has a diameter $D_{c,\,MHh}$ of 40.0 ± 1.6 m and a depth $d_{c,\,MHh}$ of 16 ± 1.9 m (Fig. 4C), where the error was derived from the validation analysis between modelling and experiments (see Section 3 and Pierazzo et al., 2008

for more details on shock codes validation). Around the crater cavity, damage occurs and might induce collapse, favouring the formation of a skylight if there were caves like lava tubes under it. The diameter of the damage area $D_{da,\ MHh}$ is about 52.7 m. The left side of Fig. 4C shows the total plastic deformation. Here, we note that, lines of deformation clearly mark the occurrence of back spallation at the rear surface.

For the case of cratering corresponding to MTh, the possible projectile is 7.2 m in diameter and the formed original crater has a diameter $D_{c,\ MTh}$ of 75.6 ± 3.0 m, and a depth $d_{c,\ MTh}$ of 30.0 ± 3.6 m. Fig. 5 exhibits the formation sequence of the crater standing at the origin of MTh. Fig. 5A represents the contact stage where a 7.2 m-diameter projectile hits the target, and Fig. 5B the end of the excavation stage. The diameter of the damage area $D_{da,\ MTh}$ is about 93.2 m (Fig. 5C).

In both MHh and MTh, the envelope of the damage areas intersects the bottom of the target (cf. Fig. 4C and 5C). This supports that the ballistic limit has been exceeded for the impact conditions of the studied hole structures, in particular the roof thicknesses. Therefore, the target-to-crater diameter (T/D_c) ratio derived from the present modelling should be smaller with respect to the Hörz (2012) one (0.7), which was instead referred to the ballistic limit. The values of the estimated diameters for the impact craters associated to MHh and MTh are used with the target thicknesses T to derive the T/D_c and D_p/T ratios considered in Hörz (2012). The target thicknesses T, which correspond to the lava tube roofs, were measured in the oblique LROC NAC images (Robinson et al., 2012), and are 26 and 47 m, respectively for MHh and MTh (cf. Fig. 2). The T/D_c ratio is 0.65 and 0.62 for MHh and MTh, respectively. As expected from the occurrence of collapse, these values are smaller than the T/Dc ratio (0.7) given in Hörz (2012) for the ballistic limit. On the other hand, in the same models, the D_p/T ratio is 0.15 for both the hole structures. In this case, we obtained a lower value than we expected. This might be accounted for the initial model setup, in particular the assumption on velocity. Afterwards, we will come back on this topic.

The present analysis has been carried out considering the target without any anisotropy. However, the real target is believed solidified magma, and hence it should exhibit planes of weaknesses that have formed during the roofing of the lava tube system. In addition, the uppermost layer is covered by a sheet of regolith that in the mare regions is typically 2–4 m (Bart et al., 2011). We performed a series of simulations, for the MHh case, considering the target to be made up by a coherent basaltic substrate, overlaid by a 3 m layer low in cohesion to reproduce the unconsolidated and fragmental nature of regolith (2.5 MPa vs. 50.0 MPa).

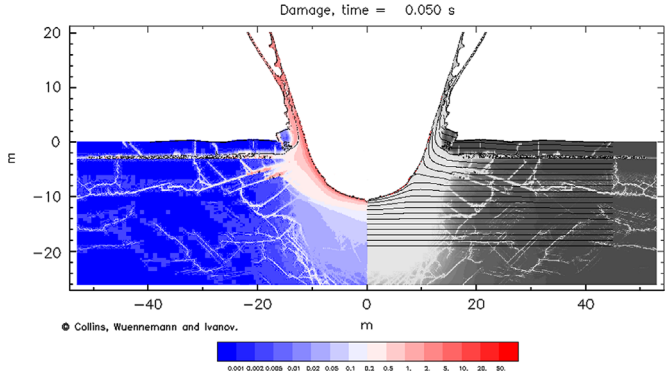

Fig. 6. Snapshot showing the end of the excavation stage of the impact crater that triggered the formation of Mare Hills hole when assuming a 26 m thick made up by a coherent basaltic substrate, overlaid by 3 m of regolith. Damage and TPS contours are shown in the right and left panel, respectively. The colour legend is the same as above. (For interpretation of the references to color in this figure legend, the reader is referred to the web version of this article.)

The cavity at the end of the excavation stage shows a complicated fracture pattern (Fig. 6), quite far from the hemispherical envelop in the previous case. The comparison of the total plastic distributions between the no-regolith (Fig. 4B) and regolith (Fig. 6) models shows highlights that the layer of damaged material inhibits the propagation of the shock front. Head et al. (2002) found that the peak spall velocity decreased with increasing thickness of the damaged layer. The same regolithic layer affects the final morphology itself, as the depth-to-diameter ratio d_c/D_c is 0.28, whereas it results 0.4 in the no-regolith case. A larger projectile, of about 6 m, turns out to better reproduce the MHh formation when introducing a regolithic upper layer. This leads to a D_p/T ratio of 0.23, which is somewhat higher of what predicted by Hörz (2012) for the laboratory impact experiments into targets without any layered structure.

A last note on the model regards the assumption on the impact velocity v_i. Our modelling was based on vertical impact geometry, but such an impact has a negligible probability to occur. In principle, impact angle and direction have a minor effect on the shape of a crater formed during a hypervelocity impact, because the final structure is primarily the result of an expanding shock wave produced during the initial contact between projectile and target (e.g., Melosh, 1989). The fact that the majority of impact craters are roughly circular in shape seems to confirm it. In addition, several studies based on either remote sensing observations or laboratory experiments have given no clear evidence to a link between structural crater asymmetry and impact angle (e.g., Poelchau and Kenkmann, 2008).

As regards MHh and MTh, they are both elliptical in shape, with a measured ellipticity of about 1.1. Laboratory experiments showed that elliptical craters are produced when impact angles are low with respect to the horizontal (e.g., Burchell and Whitehorn, 2003; Gault and Wedekind, 1978). The threshold angle depends on the target properties and impact velocity. In the case of rocks, such an angle should be about 30° (Gault and Wedekind, 1978). This means that the impact having produced these two structures might have occurred with an incidence angle below 30°. However, such impact should not necessarily have occurred at such low angle. In fact, any deviation of circularity might account also for heterogeneities (e.g., Collins et al., 2008b; Roddy, 1978) in the target, which in our case is solidified magma.

We performed a series of simulations for both the MHh and the MTh cases, with a lower impact velocity v_i, 12 km/s, which simulates an oblique impact having velocity v_i of 18 km/s and impact angle of 45°. For the MHh hole structure, a projectile with the same size of the vertical impact case (4 m) produces a crater with diameter $D_{c,\ MHh}$ of 32.4 ± 1.3 m and depth $d_{c,\ MHh}$ of 14.6 ± 1.8 m, while the damage area $D_{da,\ MHh}$ extends up to 44.8 m. This shows that to reproduce MHh with an oblique impact, a $D_p = 4.8$ m projectile is needed. In this last case, the crater has a diameter $D_{c,\ MHh}$ of 40.0 ± 1.6 m, a depth $d_{c,\ MHh}$ of 16.8 ± 2.0 m, and a damage area $D_{da,\ MHh}$ of 53.8 m. Assuming that the target thickness is 26 m, the D_p/T ratio is 0.18. For the MTh hole structure, a projectile with the same size of the vertical impact case (7.2 m) produces a crater with diameter $D_{c,\ MTh}$ of 70.4 ± 2.8 m, and depth $d_{c,\ MTh}$ of 25.6 ± 3.1 m, while the damage area $D_{da,\ MTh}$ extends up to 80.0 m. Hence, to better reproduce MTh with an oblique impact, a $D_p = 8.8$ m projectile is needed. In this last case, the crater has a diameter $D_{c,\ MTh}$ of 75.0 ± 3.0 m, a depth $d_{c,\ MTh}$ of 30.0 ± 3.6 m, and a damage area $D_{da,\ MTh}$ of 94.0 m. Assuming that the target thickness is 47 m, the D_p/T ratio is 0.19. This investigation, which adopts a lower value of the impact velocity to reproduce a 18 km/s projectile hitting the surface with an impact angle of 45°, provides more reliable values for the D_p/T ratio than

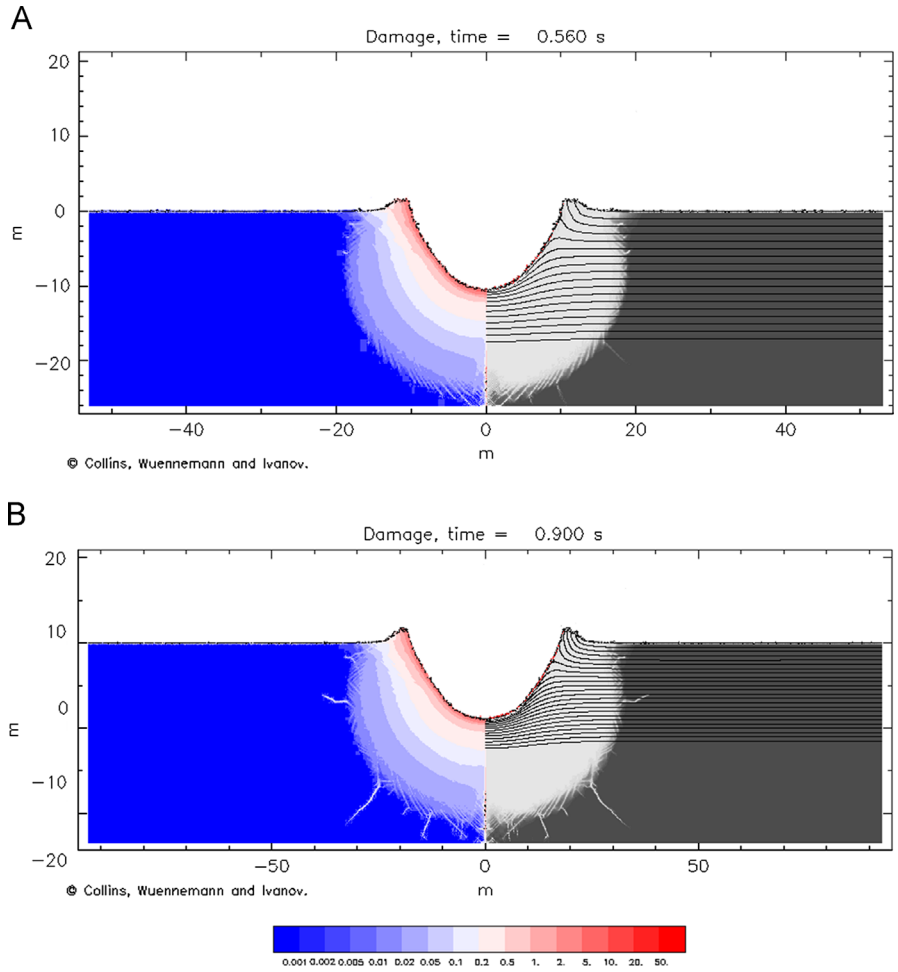

Fig. 7. This picture shows the maximum impact craters that could form without causing any subsequent collapse, in a target as thick as the estimated roof at MHh (a) and MTh (b). As in Fig. 4, the right panel shows material damage. while the left panel TPS. The colour legend is the same as above. (For interpretation of the references to color in this figure legend, the reader is referred to the web version of this article.)

the vertical impact case, when comparing to small-scale findings. This last finding seems to endorse the hypothesis of an oblique impact standing at the origin of both the hole structures.

Finally, with referring to the target thicknesses measured at MHh and MTh sites, we performed an additional suite of simulations in order to find via modelling the ballistic limit, i.e. the largest impact structures that could be sustained in the relative lava tube roofs just before perforation. The constraint was that in both cases the damage area extent would be within the target sheet and tangential to the bottom. In Fig. 7A and 7B, we show the results for the two cases.

In the MHh setting, the maximum impact crater that could form without any collapse has diameter of 23.1 ± 0.9 m, whereas in the MTh setting, the maximum impact crater has a diameter of 40.0 ± 1.6 m. These craters were obtained from an impact with a projectile of 2.4 and 4 m in diameter, respectively in the two cases. The unique fracture reaching the bottom may not be realistic because it is a line shape along the symmetry axis, and it is likely due to the axially symmetric nature of the model.

The target thickness-to-crater diameter (T/D_c) ratio results 0.89 and 0.85, respectively for MHh and MTh. These values are slightly greater than the corresponding value found in the small-scale experiments (0.7). This discrepancy was expected because we have already noticed in the former comparison that small-scale experiments slightly underestimate the T/Dc ratio with respect to modelling. On the other hand, the projectile diameter-to-target thickness (D_p/T) ratio results 0.09 and 0.08, respectively for MHh and MTh, values that are somewhat smaller than the corresponding value found in the small-scale experiments (0.16). In this case, the difference could be instead due to the initial assumption on velocity. Therefore, a future investigation throughout a 3D shock code turns to be essential to better evaluate the D_p/T ratio.

5. Conclusions

Skylights are openings on lava tubes or caves. These underground structures have been found on basaltic environments on the Earth, but also on the Moon and Mars. Lunar and Martian skylights are distinguishable to exogenic landforms because they do not display any raised rim, sloped wall, usual crater depth, or ejecta blanket.

In this paper, we investigated a possible formation mechanism of skylights associated with collapse of lava tube roofs caused by random meteoroids impacts (Hörz, 1985; Oberbeck et al., 1969), through numerical simulations with the impact Simplified Arbitrary Lagrangian Eulerian (iSALE) shock physics code.

The formation of a skylight after the collapse of an impact crater is due to the cumulative effects of the back spallation on the rear surface of a slab-like target, which corresponds to the lava tube roof. This mechanism has been examined for two gigantic lunar holes, possible skylight candidates, recently discovered on the lunar images of SELENE-Kaguya (Haruyama et al., 2009, 2010, 2012), and located in Marius Hills region and in Mare

Tranquillitatis. We firstly analysed the collapse of impact craters forming in slab-like targets, in the context of small-scale laboratory experiments available in literature.

In the numerical modelling, we considered basaltic projectiles of diameter D_p that impact at 18 km/s a basaltic coherent target of finite thicknesses T, and formed craters with rim-to-rim diameter D_c. The craters then witnessed the collapse of the surrounding damage area and developed two holes with diameter D_{da} (corresponding to the extent of the damage area). These new hole structures are proposed to be the skylight candidates observed on SELENE-Kaguya and LROC images. In the case of Marius Hills hole (MHh), a 4 m projectile impacted a 26 m thick target to form a crater with diameter $D_{c,\,MHh}$ of 40.0 ± 1.6 m, and depth of 16 ± 1.9 m. The Mare Tranquillitatis hole (MTh) was produced by a 7.2 m projectile in a 47 m thick target. The crater diameter $D_{c,\,MTh}$ is 75.6 ± 3.0 m, and the depth is 30.0 ± 3.6 m. All the depths are measured from the pre-impact surface, in conformity to the measurements presented in small-scale experiments. The T/D_c ratio results 0.65 and 0.62, respectively for MHh and MTh. These values are slightly smaller than the corresponding T/D_c ratio (0.7) given in Hörz (2012) for the ballistic limit, supporting the hypothesis that the impact craters standing at the origin of MHh and MTh exceed the ballistic limit at these sites and should collapse. The D_p/T ratio is 0.15 for both MHh and MTh. This value was expected to be higher than the Hörz (2012) D_p/T ratio (0.16), since MHh and MTh are slightly exceeding the ballistic limit. The discrepancy likely rises from the initial assumption of vertical impact. When instead adopting a lower velocity to reproduce an oblique impact by using a 2D shock code, the more reliable value of about 1.8 is obtained for the D_p/T ratio.

Finally, we derived via modelling the ballistic limit for planetary scales. The T/D_c ratio results 0.89 and 0.85, respectively for MHh and MTh, values that are slightly greater than the corresponding value found in the small-scale experiments (0.7). As expected, the D_p/T ratio results 0.09 and 0.08, respectively for MHh and MTh, values that are somewhat smaller than the corresponding value found in the small-scale experiments (0.16).

We note that the mean value of 0.87 for the T/D_c ratio obtained in this study is higher than the 0.5 proposed by Hörz (1985). This value of T/D_c should be confirmed by future work, by considering a wider range of thicknesses of lava tube and cave roofs, and evaluating systematically the effects of target layering and material properties. But, if confirmed, it implies that the number of gateways to underground structures is larger than previously thought. This could stimulate a systematic search for skylight candidates, and additional investigation to assess if they are indeed opening to lava tubes. Lava tubes were proposed as an option where future human settlements could be established to avoid the hazards on top of the lunar surface, such as the dust and radiation environments, meteoroid flux, and high temperature gradient. However, habitat and laboratory infrastructures should be accordingly deployed at some distance to the skylight itself, to avoid possible subsequent collapse related to the same mechanism that formed the hole structure.

A phased approach for surface and subsurface exploration is recommended by ILEWG (e.g., Foing et al., 2008a, 2008b) and COSPAR (Ehrenfreund et al., 2012). This implies a first detailed and comprehensive analysis of data from previous missions to describe the general context where sinuous rilles form and can lead to lava tubes using data at medium resolution (e.g., SMART-1, see Foing et al., 2006), and a survey of skylights at sub-metric resolution (LRO, Robinson et al., 2010). Further investigations, such as radar mapping from orbit, surface surveys with rovers equipped with Ground Penetrating Radar (GPR), and tomographic seismic techniques are needed to consider the feasibility of using lava tubes as settlements of human bases on the Moon.

Acknowledgements

We gratefully acknowledge the developers of iSALE, including Gareth Collins, Kai Wünnemann, Boris Ivanov, Jay H. Melosh, and Dirk Elbeshausen (see www.iSALE-code.de).

We are very grateful to F. Marzari and M. Massironi for helpful comments that improved our manuscript. We are also grateful to D. Loizeau and J. Haruyama for constructive discussions. The manuscript was significantly improved by the comments from an anonymous reviewer.

This paper is a result of a work supported by the European Space Agency (ESA) (contract no. ESA/YG-ESTEC(2010)015).

References

Amsden, A.A., Ruppel, H.M., Hirt, C.W., 1980. Sale: A Simplified ALE Computer Programme for Fluid Flows at all Speeds. Los Alamos National Laboratories, Report LA-8095.

Anderson Jr., C.E., 1987. An overview of the theory of hydrocodes. International Journal of Impact Engineering 5, 33–59.

Bart, G.D., Nickerson, R.D., Lawder, M.T., Melosh, H.J., 2011. Global survey of lunar regolith depths from LROC images. Icarus 215, 485–490.

Barton, H.A., 2006. Introduction to cave microbiology: a review for the non-specialist. Journal of Cave and Karst Studies 68, 43–54.

Boston, P.J., Ivanov, M.V., McKay, C.P., 1992. On the possibility of chemosynthetic ecosystem in subsurface habitats on mars. Icarus 95, 300–308.

Britt, D.T., Yeomans, D., Housen, K.R., Consolomagno, G., 2002. Asteroid density, porosity and structure. In: Bottke W.K., Jr., Cellino, P., Paolicchi, P., Binzel, R.P. (Eds.), Asteroids III. Univ. Arizona Press, Tucson, pp. 485–500.

Burchell, M.J., Whitehorn, L., 2003. Oblique incidence hypervelocity impacts on rocks. Monthly Notices of the Royal Astronomical Society 341, 192–198.

Burchell, M.J., Robin-Williams, R., Foing, B.H., 2010. The SMART-1 lunar impact. Icarus 207, 28–38.

Calvari, S., Pinkerton, H., 1998. Formation of lava tubes and extensive flow field during the 1991–1993 eruption on Mount Etna. Journal of Geophysical Research 103, 27,291–27,301.

Calvari, S., Pinkerton, H., 1999. Lava tube morphology on Etna and evidence for lava flow emplacement mechanisms. Journal of Volcanology and Geothermal Research 90, 263–280.

Chyba, C.F., 1991. Terrestrial mantle siderophiles and the lunar impact record. Icarus 92, 217–233.

Collins, G.S., Melosh, H.J., Morgan, J.V., Warner, M.R., 2002. Hydrocodes simulations of Chicxulub crater collapse and peak–ring formation. Icarus 157, 24–33.

Collins, G.S., Melosh, H.J., Ivanov, B.A., 2004. Modelling damage and deformation in impact simulations. Meteoritics and Planetary Science 39, 217–231.

Collins, G.S., Morgan, J., Barton, P., Christeson, G.L., Gulick, S., Urrutia, J., Warner, M., Wünnemann, K., 2008a. Dynamic modeling suggests terrace zone asymmetry in the Chicxulub crater is caused by target heterogeneity. Earth and Planetary Science Letters 270, 221–230.

Collins, G.S., Kenkmann, T., Osinski, G.R., Wünnemann, K., 2008b. Mid-sized complex crater formation in mixed crystalline-sedimentary targets: Insight from modelling and observation. Meteoritics and Planetary Science 43, 1955–1977.

Collins, G.S., Elbeshausen, D., Davison, T.M., Robbins, S.J., Hynek, B.M., 2011a. The size-frequency distribution of elliptical impact craters. Earth and Planetary Science Letters 310, 1–8.

Collins, G.S., Melosh, H.J., Wünnemann, K., 2011b. Improvements to the ε–α porous compaction model for simulating impacts into high-porosity solar system objects. International Journal of Impact Engineering 38, 434–439.

Coombs, C.R., Hawke, B.R., 1992. A search for intact lava tubes on the Moon: possible lunar base habitats. In: Proceedings of the Second Conference on Lunar Bases and Space Activities of the 21st Century, vol. 1. SEE N93-17414 05-91. NASA, Johnson Space Center, pp. 219–229.

Cruikshank, D.P., Wood, C.A., 1972. Lunar Rilles and Hawaiian volcanic features: possible anologues. The Moon 3, 412–447.

Cushing, G.E., Titus, T.N., Wynne, J.J., Christensen, P.R., 2007. THEMIS observes possible cave skylights on Mars. Geophysical Research Letters 34, L17201.

Davison, L., Graham, R.A., 1979. Shock compression of solids. Physics Reports 4, 255–379.

Davison, T., Collins, G.S., Ciesla, F.J., 2010. Numerical modelling of heating in porous planetesimal collisions. Icarus 208, 468–481.

Dufresne, A., Poelchau, M.H., Kenkmann, T., Deutsch, A., Hoerth, T., Schäfer, F., Thoma, K., 2013. Crater morphology in sandstone targets: The MEMIN impact parameter study. Meteoritics and Planetary Science 48, 50–70.

Ehrenfreund, P., McKay, C., Rummel, J.D., Foing, B.H., Neal, C.R., Masson-Zwaan, T., Ansdell, M., Peter, N., Zarnecki, J., Mackwell, S., Perino, M.A., Billings, L., Mankins, J., Race, M., 2012. Toward a global space exploration programme: a stepping stone approach. Advances in Space Research 49, 2–48.

Elbeshausen, D., Wünnemann, K., Collins, G.S., 2009. Scaling of oblique impacts in frictional targets: implications for crater size and formation mechanisms. Icarus 204, 716–731.

Foing, B.H., Racca, G.D., Marini, A., Evrard, E., Stagnaro, L., Almeida, M., Koschny, D., Frew, D., Zender, J., Heather, J., Grande, M., Huovelin, J., Keller, H.U., Nathues, A., Josset, J.L., Malkki, A., Schmidt, W., Noci, G., Birkl, R., Iess, L., Sodnik, Z., Mcmanamon, P., 2006. SMART-1 mission to the Moon: status, first results and goals. Advances in Space Research 37, 6–13.

Foing, B.H., Ehrenfreund, P., 2008a. Journey to the Moon: recent results, science, future robotic and human exploration. Advances in Space Research 42, 235–237.

Foing, B.H., International Lunar Exploration Working Group, 2008b. Report from ILEWG to the Lunar Science Workshop 2008. In: Proceedings of the NLSI Lunar Science Conference, July 20–23, 2008, NASA Ames Research Center, Moffett Field, California, LPI Contribution No. 1415, Abstract no. 2090.

French, B.M., 1998. Traces of Catastrophe: A Handbook of Shock–Metamorphic Effects in Terrestrial Meteorite Impact Structures. LPI Contribution No. 954. Lunar & Planetary Institute, Houston p. 120.

Fujiwara, A., 1980. On the mechanism of catastrophic destruction of minor planets by high-velocity impact. Icarus 41, 356–364.

Gault, D.E., Wedekind, J.A., 1978. Experimental studies of oblique impact. In: Proceedings of the 9th Lunar Planetary Science Conference, pp. 3843–3875.

Gehring jr, J.W., 1970. Engineering considerations in hypervelocity impact. In: Kinslow, R. (Ed.), High Velocity Impact Phenomena. Academic Press, New York, pp. 463–514.

Gillis-Davis, J.J., Blewett, D.T., Gaskell, R.W., Denevi, B.W., Robinson, M.S., Strom, R.G., Solomon, S.C., Sprague, A.L., 2009. Pit-floor craters on Mercury: evidence of near-surface igneous activity. Earth and Planetary Science Letters 285, 243–250.

Greeley, R., 1970. Terrestrial analogs to lunar dimple (drainage) craters. The Moon 1, 237–252.

Greeley, R., 1971. Lava tubes and channels in the lunar marius hills. The Moon 3, 289–314.

Greeley, R., 1987. The role of lava tubes in Hawaiian volcanoes. In: Volcanism in Hawaii, U.S. Geological Survey Prof. Paper 1350, pp. 1589–1602.

Greeley, R., Gault, D.E., 1979. Endogenic craters on basaltic lava flows–size frequency distributions. In: Proceedings of the 10th Lunar Planetary Science Conference, pp. 2919–2933.

Grieve, R.A.F., Garvin, J.B., Coderre, J.M., Rupert, J., 1989. Test of a geometric model for the modification stage of simple impact crater development. Meteoritics 24, 83–88.

Haruyama, J., Hioki, K., Shirao, M., Morota, T., Hiesinger, H., van der Bogert, C.H., Miyamoto, H., Iwasaki, A., Yokota, Y., Ohtake, M., Matsunaga, T., Hara, S., Nakanotani, S., Pieters, C.M., 2009. Possible lunar lava tube skylight observed by SELENE cameras. Geophysical Research Letters 36, L21206.

Haruyama, J., Hara, S., Hioki, K., Morota, T., Yokota, Y., Shirao, M., Hiesinger, H., van der Bogert, C.H., Miyamoto, H., Iwasaki, A., Ohtake, M., Saito, Y., Matsunaga, T., Nakanotani, S., Pieters, C.M., Lucey, P.G., 2010. New discoveries of Lunar holes in Mare Tranquillitatis and Mare Ingenii. In: Proceedings of the 41st LPSC, March 1–5, 2010, The Woodlands, Texas, LPI Contribution no. 1533, pp. 1285.

Haruyama, J., Morota, T., Kobayashi, S., Sawai, S., Lucey, P.G., Shirao, M., Nishino, M.N., 2012. Lunar Holes and Lava Tubes as Resources for Lunar Science and Exploration. In: Badescu, V. (Ed.), Moon–Prospective Energy and Material Resources. Springer, pp. 139–164.

Head, J.N., Melosh, J.H., Ivanov, B.A., 2002. Martian meteorite launch: high-speed ejecta from small craters. Science 298, 1752–1756.

Holsapple, K.A., Housen, K.R., 2007. A crater and its ejecta: an interpretation of deep impact. Icarus 187, 345–356.

Hörz, F., 1985. Lava tubes: potential shelters for habitats, in: Lunar bases and space activities of the 21st century (A86-30113 13-14). Lunar and Planetary Institute, Houston, TX, pp. 405–412.

Hörz, F., 2012. Cratering and penetration experiments in aluminium and teflon: Implications for space-exposed surfaces. Meteoritics and Planetary Science 47, 763–797.

Hörz, F., Cintala, M.J., Bernhard, R.P., See, T.H., 1995. Cratering and penetration experiments in teflon targets at velocities from 1 to 7 km/s. International Journal of Impact Engineering 17, 419–430.

Huang, Q., Wieczorek, M.A., 2012. Density and porosity of the lunar crust from gravity and topography. Journal of Geophysical Research 117, E05003.

Ivanov, B.A., 2005. Numerical modeling of the largest terrestrial meteorite craters. Solar System Research 39, 381–409.

Ivanov, B.A., Artemieva, N., 2002. Numerical modeling of the formation of large impact craters. In: Koeberl, C., MacLeod, K.G. (Eds.), Impact and Beyond, Geol. Sci. Am. Sp. Pap, 356. Catastrophic Events and Mass Extinctions, pp. 619–630.

Ivanov, B.A., Deniem, D., Neukum, G., 1997. Implementation of dynamic strength models into 2D hydrocodes: application for atmospheric breakup and impact cratering. International Journal of Impact Engineering 20, 411–430.

Johnson, J.N., 1981. Dynamic fracture and spallation in ductile solids. Journal of Applied Physics 52, 2812–2825.

Kenkmann, T., Ivanov, B.A., 2006. Target delamination by spallation and ejecta dragging: An example from the Ries crater's periphery. Earth and Planetary Science Letters 252, 15–29.

Kenkmann, T., Wünnemann, K., Deutsch, A., Poelchau, M.H., Schäfer, F., Thoma, K., 2011. Impact cratering morphology in sandstone: the MEMIN pilot study on the effect of pore water. Meteoritics and Planetary Science 46, 890–902.

Keszthelyi, L., 1995. A preliminary thermal budget for lava tubes on the Earth and planets. Geophysical Research 100, 20,411–20,420.

Korycansky, D.G., Plesko, C.S., Jutzi, M., Asphaug, E., Colaprete, A., 2009. Predictions for the LCROSS mission. Meteoritics and Planetary Science 44, 603–620.

Léveillé, R.J., Datta, S., 2010. Lava tubes and basaltic caves as astrobiological targets on Earth and Mars: a review. Planetary and Space Science 58, 592–598.

Levy, D.H., 1998. The collision of comet shoemaker-levy 9 with Jupiter. Space Science Reviews 85, 523–545.

Love, S.G., Hörz, F., Brownlee, D.E., 1993. Target porosity effects in impact cratering and collisional disruption. Icarus 105, 216–224.

Marchi, S., Mottola, S., Cremonese, G., Massironi, M., Martellato, E., 2009. A new chronology for the Moon and Mercury. The Astronomical Journal 137, 4936–4948.

Melosh, H.J., 1984. Impact ejection, spallation, and the origin of meteorites. Icarus 59, 234–260.

Melosh, H.J., 1989. Impact Cratering: A Geologic Process. Oxford University Press, New York p. 245.

Melosh, H.J., Ryan, E.V., Asphaug, E., 1992. Dynamic Fragmentation in Impact: Hydrocode Simulation of Laboratory Impacts. Journal of Geophysical Research 97, 14,735–14,759.

Melosh, H.J., Ivanov, B.A., 1999. Impact crater collapse. Annual Review of Earth and Planetary Sciences 27, 385–415.

Oberbeck, V.R., Quaide, W.L., Greeley, R., 1969. On the origin of lunar sinuous rilles. Modern Geology 1, 75–80.

Okubo, C.H., Martel, S.J., 1998. Pit crater formation on Kilauea volcano, Hawaii. Journal of Volcanology and Geothermal Research 86, 1–18.

Pierazzo, E., Chyba, C.F., 1999. Amino acid survival in large cometary impacts. Meteoritics and Planetary Science 34, 909–918.

Pierazzo, E., Collins, G.S., 2004. A brief introduction to hydrocode modelling. In: Dypvik, H., Burchell, M.J., Claeys, P. (Eds.), Cratering in Marine Environments and on Ice. Springer, Verlag, Berlin, pp. 323–340.

Pierazzo, E., Artemieva, N., Asphaug, E., Baldwin, E.C., Cazamias, J., Coker, R., Collins, G.S., Crawford, D.A., Davison, T., Elbeshausen, D., Holsapple, K.A., Housen., K.R., Korycansky, D.G., Wünnemann, K., 2008. Validation of numerical codes for impact and explosion cratering: Impacts on strengthless and metal targets. Meteoritics and Planetary Science 43, 1917–1938.

Poelchau, M.H., Kenkmann, T., 2008. Asymmetric signatures in simple craters as an indicator for an oblique impact direction. Meteoritics and Planetary Science 43, 2059–2072.

Poelchau, M.H., Kenkmann, T., Thoma, K., Hoerth, T., Dufresne, A., Schäfer, F., 2013. Meteoritics and Planetary Science 48, 8–22.

Polanskey, C.A., Ahrens, T.J., 1990. Impact spallation experiments–fracture patterns and spall velocities. Icarus 87, 140–155.

Rice, J.R., 1976. The localization of plastic deformation. In: Proceedings of the 14th International Conference on Mechanical Engineering, pp. 207–220.

Richardson jr, J.E., Melosh, H.J., Artemieva, N.A., Pierazzo, E., 2005. Impact cratering theory and modeling for the Deep Impact mission: from mission planning to data analysis. Space Science Reviews 117, 241–267.

Robinson, M.S., Brylow, S.M., Tschimmel, M., Humm, D., Lawrence, S.J., Thomas, P.C., Denevi, B.W., Bowman-Cisneros, E., Zerr, J., Ravine, M.A., Caplinger, M.A., Ghaemi, F.T., Schaffner, J.A., Malin, M.C., Mahanti, P., Bartels, A., Anderson, J., Tran, T.N., Eliason, E.M., McEwen, A.S., Turtle, E., Jolliff, B.L., Hiesinger, H., 2010. Lunar Reconnaissance Orbiter Camera (LROC) instrument overview. Space Science Reviews 150, 81–124.

Robinson, M.S., Ashley, J.W., Boyd, A.K., Wagner, R.V., Speyerer, E.J., Ray Hawke, B., Hiesinger, H., van der Bogert, C.H., 2012. Confirmation of sublunarean voids and thin layer in mare deposits. Planetary and Space Science 69, 18–27.

Roddy, D.J., 1978. Pre-Impact conditions and cratering processes at meteor crater, Arizona, a typical bowl-shaped crater. In: Proceedings of the 9th Lunar and Planetary Science Conference, pp. 3891–3930.

Schultz, P.H., Hermalyn, B., Colaprete, A., Ennico, K., Shirley, M., Marshall, W.S., 2010. The LCROSS Cratering Experiment. Science 330, 468–472.

Shoemaker, E.M., 1962. Interpretation of lunar craters. In: Kopal, Z. (Ed.), Physics and Astronomy of the Moon. Academic, New York, pp. 283–359.

Thompson, S.L., 1970. Improvements in the CHART-D radiation hydrodynamic code I: Analytical equation of state. Sandia National Laboratories, Report SC-RR 70-28.

Thompson, S.L., Lauson, H.S., 1972. Improvements in the CHART-D radiation-hydrodynamic code III: Revised analytical equation of state. Sandia National Laboratories, Report SC-RR-710714.

Tillotson, J.H., 1962. Metallic equations of state for hypervelocity impact, General Atomic, Report GA-3216.

Wentworth, C.K., MacDonald, G.A., 1953. Structures and forms of basaltic rocks in Hawaii 994 98 US Geological Survey Bulletin 994, 98p.

Wünnemann, K., Lange, M.A., 2002. Numerical modelling of impact–induced modifications of the deep–sea floor. Deep Sea–Research Part II 49, 969–982.

Wünnemann, K., Ivanov, B.A., 2003. Numerical modelling of the impact crater depth–diameter dependence in an acoustically fluidized target. Solar System Research 51, 831–845.

Wünnemann, K., Morgan, J.V., Jödicke, H., 2005. Is ries crater typical for its size? An analysis based upon old and new geophysical data and numerical modeling. In: Kenkman, T., Hörz, F., Deutsch, A. (Eds.), Large Meteorite Impacts III, Geological Society of America, pp. 67–83.

Wünnemann, K., Collins, G.S., Melosh, H.J., 2006. A strain-based porosity model for use in hydrocode simulations of impacts and implications for transient crater growth in porous targets. Icarus 180, 514–527.

Wyrick, D., Ferrill, D.A., Morris, A.P., Colton, S.L., Sims, D.W., 2004. Distribution, morphology, and origins of Martian pit crater chains. Journal of Geophysical Research 109, E06005.